

www.acsnano.org

# Identification of Brillouin Zones by In-Plane Lasing from Light-Cone Surface Lattice Resonances

Jun Guan, Marc R. Bourgeois, Ran Li, Jingtian Hu, Richard D. Schaller, George C. Schatz,\* and Teri W. Odom\*



Cite This: ACS Nano 2021, 15, 5567-5573



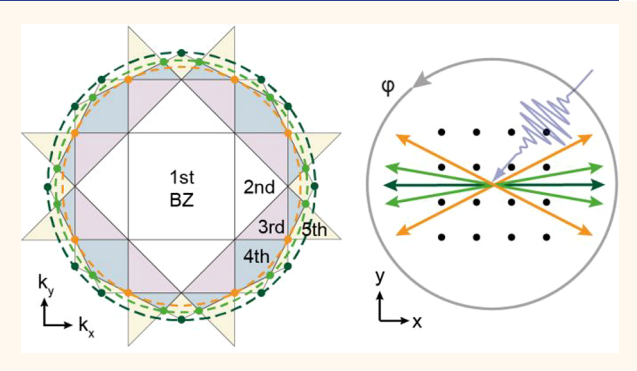
**ACCESS** I

III Metrics & More

Article Recommendations

s Supporting Information

ABSTRACT: Because of translational symmetry, electromagnetic fields confined within 2D periodic optical structures can be represented within the first Brillouin zone (BZ). In contrast, the wavevectors of scattered electromagnetic fields outside the lattice are constrained by the 3D light cone, the free-photon dispersion in the surrounding medium. Here, we report that light-cone surface lattice resonances (SLRs) from plasmonic nanoparticle lattices can be used to observe the radiated electromagnetic fields from extended BZ edges. Our coupled dipole radiation theory reveals how lattice geometry and induced surface plasmon dipole orientation affect angular distributions of the radiated fields. Using dye molecules as local dipole emitters to excite the light-



cone SLR modes, we experimentally identified high-order BZ edges by directional, in-plane lasing emission. These results provide insight into nanolaser architectures that can emit at multiple wavelengths and in-plane directions simply by rotating the nanocavity lattice.

KEYWORDS: light-cone surface lattice resonance, plasmon nanolaser, metal nanoparticle lattice, photonic Brillouin zone, radiative loss, coupled dipole radiation theory

and structure engineering enables control over electronic and optical properties of periodic materials. <sup>1,2</sup> Because of the discrete translational symmetry of an atomic crystal, the first Brillouin zone (BZ) in reciprocal space can fully describe the electronic eigenstates and inclusive properties. <sup>3,4</sup> In contrast to electrons bound in a solid, photons in a periodic optical structure can couple to far-field radiation, <sup>4</sup> and characteristics of the radiated photons, including the direction, intensity, phase, and polarization, cannot be fully represented by the first BZ. The free-photon dispersion relation in a surrounding medium imposes an upper bound on the magnitude of the wavevectors of photonic modes that can interact with external fields; <sup>2,5</sup> this constraint for two-dimensional (2D) optical modes is denoted as the *light cone*.

For example, because the dispersion relation of surface plasmon polaritons (SPPs) on a flat metal surface is beyond the light cone, additional momentum in the form of a periodic grating or via a Kretschmann configuration is required to excite SPPs with an external electromagnetic field.<sup>6,7</sup> Different from SPPs, the dispersion of dielectric photonic lattices often resides within the light cone; <sup>8–12</sup> Lorentz reciprocity states that since photonic lattices can be excited by external light, they can also

radiate light into the far field via scattering, which results in radiative loss. Photonic modes consist of both localized fields inside the lattice and radiated fields in the surroundings. To connect the external radiated fields with the localized fields, extended BZ schemes that include the first and higher order BZs within the light cone must be considered. In addition, since Maxwell's equations are vectorial, investigations of how the vector nature of the electromagnetic fields affects radiative losses of periodic structures are needed. However, these studies have been limited due to the lack of materials systems that can facilitate both light trapping and strong scattering.

Plasmonic nanoparticles arranged in a periodic array support surface lattice resonances (SLRs) arising from the coupling of localized surface plasmons (LSPs) and diffraction modes.<sup>13–16</sup>

Received: January 16, 2021 Accepted: March 3, 2021 Published: March 9, 2021





Because plasmonic nanoparticles allow deep-subwavelength light confinement and also serve as far-field scatterers, <sup>15,16</sup> the SLR platform can provide both concentrated local fields near the nanoparticles and strong radiation intensities outside the lattice. Integrating gain media with nanoparticle lattices can result in nanoscale lasing, <sup>17–19</sup> where the high local density of optical states at the band edges provides optical feedback and the corresponding in-plane wavevectors of the band-edge states determine the emission angles. Lasing action can be used as an effective diagnostic tool to visualize the high-symmetry points of plasmonic lattices. <sup>20–22</sup>

In this paper, we show that SLR modes on the light cone enable the identification of photonic BZ edges. We demonstrate that projecting the light cone onto 2D extended BZs provides a method for predicting the energies and spatial directions at which electromagnetic fields are scattered into 3D surroundings. To validate this geometric construction, we developed a coupled dipole radiation theory that reveals how lattice geometry as well as electric dipole orientation determine the spatial distribution of the radiated electromagnetic fields. Using dye molecules as local excitation sources, we experimentally probed the BZ edges of square lattices of aluminum nanoparticles by observing their lasing characteristics. By accessing the third through the fifth BZ edges, we also demonstrated the azimuthal dependence of in-plane lasing at different wavelengths by simply rotating the lattice.

#### **RESULTS AND DISCUSSION**

Figure 1a depicts the projection of the light cone on BZs for square nanoparticle lattices with two different periodicities ( $a_0$ 

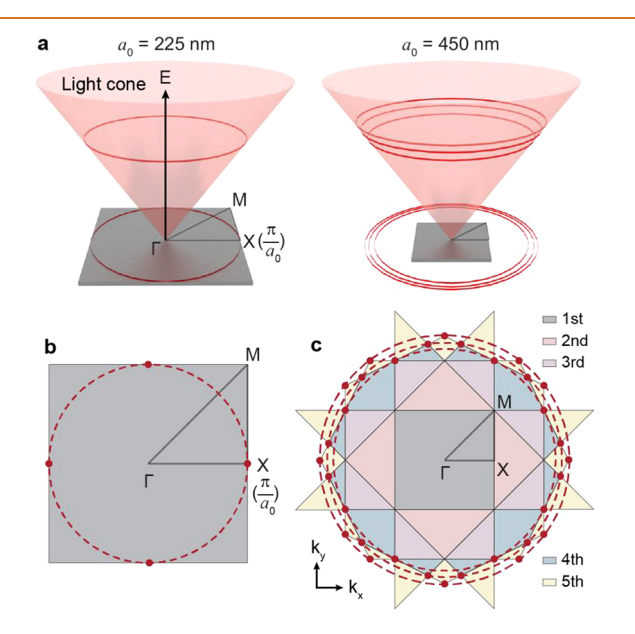


Figure 1. Projection of the light cone on extended BZs enables prediction of light-cone SLR modes. (a) Scheme of a light cone in k-space, and the projection on the reciprocal space of the 2D lattice. The three circles in the  $a_0=450$  nm result refer to three choices of emission wavelength, as used in later plots. (b) Design of light-cone SLR modes at the X point of the first BZ. The gray square indicates the first BZ. The red dashed circle indicates the cross section of the light-cone boundary. The red dots show the light-cone SLR modes. (c) Design of light-cone SLR modes at the third to the fifth BZ edges. The colored areas indicate the first (1st) to the fifth (5th) BZs.

= 225 and 450 nm). The 3D light-cone boundary in the 2D E- $\mathbf{k}_{\parallel}$  relation corresponds to  $\theta = 90^{\circ}$  in the  $\lambda - (\theta, \varphi)$  angle description, which means that the radiated light is constrained to be in the plane of the lattice (Figure S1). Circular cross sections of the light cone indicate the maximum in-plane wavevector magnitude at a given photon energy, and intersecting wavevectors of BZ edges represent the in-plane direction of the photon radiation. Because the SLR modes in plasmonic nanoparticle lattices are LSP-dressed Bragg diffraction modes, i.e., lattice plasmon polaritons, the optical band structure closely resembles the free-photon band structure dictated by the lattice geometry.<sup>23</sup> The empty-lattice dispersion relation is  $|\mathbf{k}_{\parallel} + \mathbf{G}| = n \frac{E}{\hbar c}$ , where  $\mathbf{k}_{\parallel}$  is the wavevector component parallel to the lattice plane, G is a reciprocal lattice vector, *n* is the refractive index of the environment, and *E* is the photon energy. Since G is defined as  $G = m_1b_1 + m_2b_2$  where b<sub>1</sub> and b<sub>2</sub> are the primitive vectors of the reciprocal lattice and  $m_1, m_2 \in \mathbb{Z}$ , the light-cone boundary can be interpreted as a G = (0, 0) diffraction mode in the lattice (Figure S1). We define light-cone SLR modes as band-edge SLR modes located on the light-cone boundary that result from interference between the G = (0, 0) mode with other diffraction modes and where the radiated light is in-plane.

With lattice periodicity  $a_0 = 225$  nm, we investigated first BZ boundaries by light-cone SLR modes at the X point (Figure 1b). Based on the empty-lattice approximation, 23,24 the lowest energy band-edge mode occurs at the crossing of (1, 0) and (0, 0)0) diffraction orders at the X point (Figure S1). The resonance wavelength is at visible wavelengths near the diffraction condition  $\lambda = 2a_0 \times n$ , where  $a_0 = 225$  nm is the lattice periodicity, and n = 1.45 is the refractive index of the environment. Projection of the light-cone boundary on the first BZ provides a simple geometric approach to predict the radiation properties of light-cone SLR modes: (1) the slope of the light-cone boundary is proportional to n; (2) the shape and size of the BZ indicate the lattice geometry and periodicity  $a_0$ , respectively; and (3) the energies and wavevectors occur at the intersection of light-cone boundary projected on the BZ. For example, at the X points in the first BZ, the four intersections in k-space denote in-plane light radiation along the  $\pm x$  and the  $\pm$  y directions (Figure 1b, red dots).

We increased the lattice periodicity in real space ( $a_0 = 450$ nm) to reduce the sizes of all the BZs in reciprocal space so that the third to the fifth BZ boundaries are at visible wavelengths (Figure 1c). The nth BZ is defined as the set of points that can be reached from the origin of the reciprocal lattice by passing through the (n-1)th Bragg plane; each BZ is a valid primitive unit cell of the reciprocal lattice.<sup>3</sup> The BZ edges correspond to the degenerate points of the Bragg diffraction orders where band-edge SLR modes appear. At these BZ edges, three sets of light-cone SLR modes are observed and whose energies are proportional to the radii of the light-cone cross sections (Figure 1c, dashed red lines). Since the high-order BZs have more complicated symmetries compared to that of the first BZ, the radiated photons at these light-cone SLR modes are along multiple (8, 12, and 12) inplane directions characterized by different azimuthal angles. Compared to geometric methods based on reciprocal lattice points<sup>25</sup> and wavevector diagrams,<sup>12</sup> our approach can (1) capture all the band-edge states in a photonic lattice of any geometry and (2) predict the energies and wavevectors of

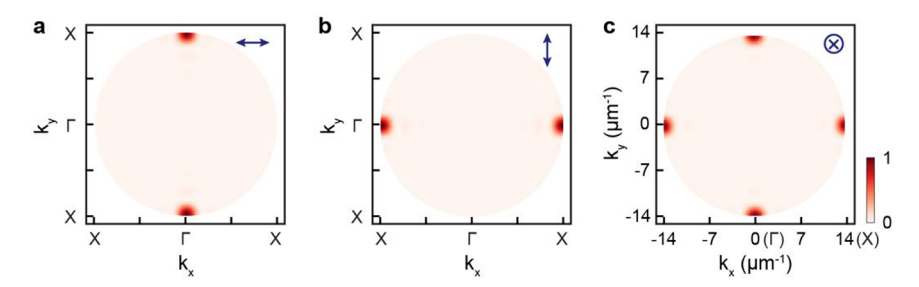


Figure 2. Radiation intensity can be manipulated by the dipole orientation because of the vector nature of electromagnetic fields. Calculated radiation intensity distributions at the X point of the  $a_0 = 225$  nm lattice with (a) x-, (b) y-, and (c) z-polarized dipole moments. The unit of the intensity is  $\frac{\sqrt{\varepsilon_r}\omega^4 \mid p\mid^2}{32\pi^2\varepsilon_0c^3N^2}$ .

band-edge states from the geometry of extended BZs without needing to solve any analytical equations.

To confirm that this geometric construction can determine angular distributions of the radiated electromagnetic fields from light-cone SLR modes, we developed a coupled dipole radiation theory to separate out contributions from lattice geometry and dipole orientation (Supporting Information Section 2, Figure S2). Far away from the lattice, the radiated intensity distribution per lattice site  $I(\mathbf{k})$  from a D-dimensional (D = 1, 2, 3) lattice of any geometry can be expressed as

$$I(\mathbf{k}) = \frac{\sqrt{\varepsilon_r}\omega^4}{32\pi^2\varepsilon_0c^3N^2} |(\vec{I} - \hat{\mathbf{k}}\hat{\mathbf{k}})\cdot\mathbf{p}|^2 \left| \prod_{j=1}^D \frac{\sin\left(\frac{N_j(\mathbf{k} - \mathbf{K})\cdot\mathbf{a}_j}{2}\right)}{\sin\left(\frac{(\mathbf{k} - \mathbf{K})\cdot\mathbf{a}_j}{2}\right)} \right|^2$$

where  $a_i$  are the primitive vectors, p is the dipole moment of a single nanoparticle, k is the wavevector of the radiated fields, K is the Bloch vector in the lattice,  $N_i$  is the number of nanoparticles along the  $a_i$  direction, and N the total number of nanoparticles in the lattice. Our theory reveals that the lattice geometry determines the radiation direction and that the electric dipole orientation determines the radiation amplitude. Unlike scalar structure factors that describe the scattering intensities of atomic crystals, 3,26 in photonic lattices, the structure factor  $S = (\vec{l} - \hat{k}\hat{k}) \cdot p$  is a vector and depends on the vectorial nature (e.g. orientation) of the electric dipole. This difference arises because photonic systems exhibit vector eigenstates, while electronic wave functions are scalar valued. Our theory also shows that the arrangement of electric dipoles in non-Bravais lattices can manipulate the interference of radiated light and thus intensity distributions (Supporting Information Section 2).

Using the X point in the first BZ of the  $a_0$ = 225 nm array as an example, we demonstrate how dipole orientation affects the radiation intensity distributions (Figure 2, Figure S3). To include radiated fields from all possible SLR modes, we sum over the electric fields from all wavevectors  $\mathbf{k}_{\parallel}$  within the first BZ with dipole LSPs orientated along the x, y, and z directions, respectively. Our calculations confirm that the emission is inplane and show that although diffraction directions are determined by lattice geometry, the dipole orientations can fully suppress radiation intensities along certain directions through destructive interference of the radiated photons.

We experimentally evaluated the first BZ boundary of 2D square arrays of aluminum nanoparticles. These lattices were fabricated on fused silica using solvent-assisted nanoscale embossing (SANE<sup>27</sup>) and PEEL processes<sup>28,29</sup> ( $a_0 = 225$  nm, diameter d = 70 nm, height h = 60 nm) (Figure 3a). A droplet

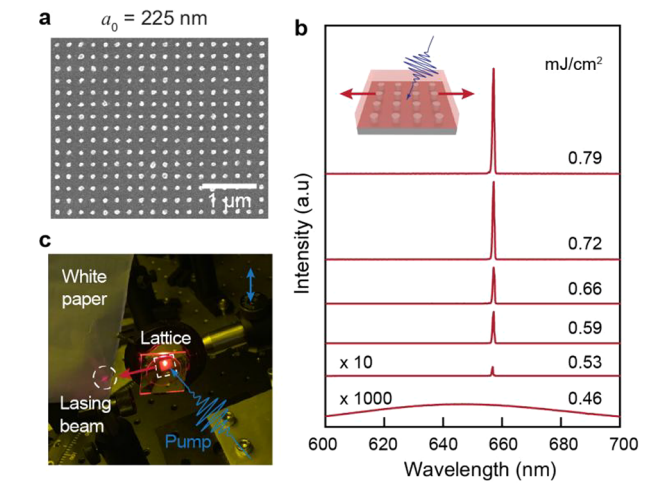


Figure 3. Identification of 1st BZ using dye molecules as local dipole excitation sources. (a) Scanning electron microscope image of aluminum nanoparticle lattices. (b) Power-dependent lasing spectra. Inset depicts a scheme of the directions of lasing emission. (c) Photo of the lasing beam emitted parallel and along the lattice plane. The blue arrow shows the polarization direction of the pump laser. The red arrow shows the lasing emission direction.

of DCM-DMSO solution (5 mM; photoluminescence bandwidth: 615-685 nm) was placed on the nanoparticle lattice so that the dye molecules excited by a 400 nm fs pulsed laser served as local probes of the light-cone SLR modes. The transition dipole orientations of the molecules determine the excited dipoles of the plasmonic nanoparticles, 30,31 and the lasing emission direction of the dyes indicate the radiation properties of the light-cone SLR modes. Because the dye concentration is low (5 mM), there is only weak coupling between dye molecules and the plasmonic nanoparticle lattice; 16,17 the SLR band structure is not modified. At low pump intensities (<0.5 mJ/cm<sup>2</sup>), only a broad photoluminescence profile (full-width half-maximum (fwhm) ~ 70 nm) was observed, and the spontaneous emission exhibited no spatial directionality (Figure 3b, Figure S4). Above a critical pump intensity (>0.5 mJ/cm<sup>2</sup>), a narrow, intense peak above background ( $\lambda$  = 657 nm, fwhm ~0.5 nm) emerged, which is characteristic of coherent photon emission, where optical feedback is provided by highly confined electromagnetic fields near the nanoparticles. 17 The in-plane lasing beams were visualized on a piece of white paper placed at the edge of the sample, where the far-field emission directions along  $\pm x$ directions (Figure 3c) show a signature of the X point in the first BZ (Figures 1b and 2b). We note that although the in-

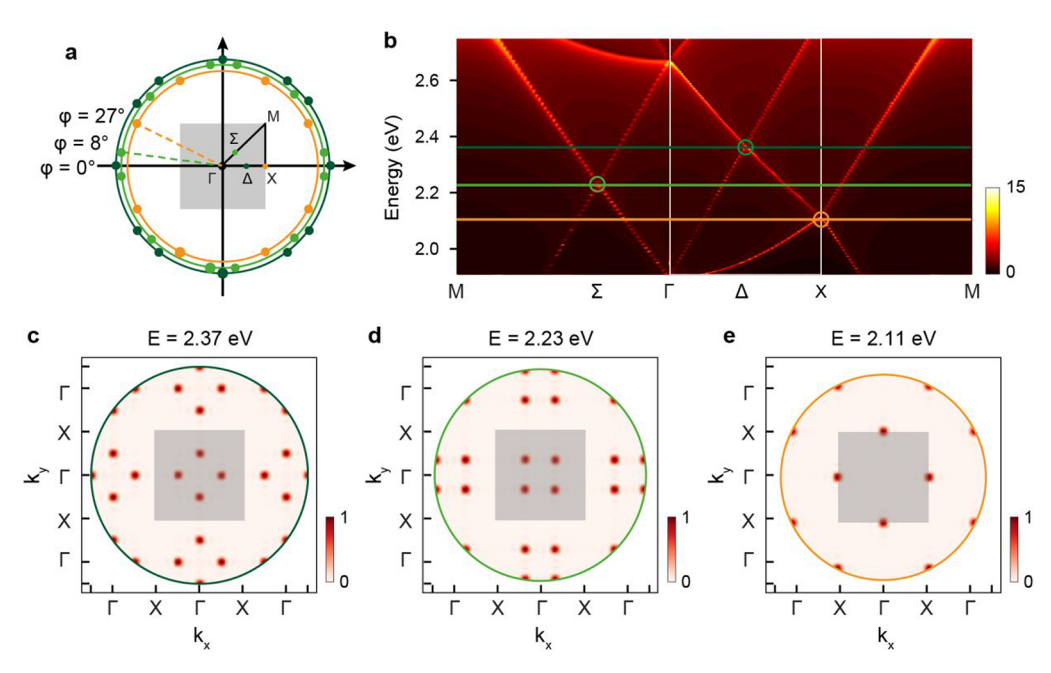


Figure 4. Geometry of extended BZs enables multiple band-edge modes along different lattice directions. (a) Design of light-cone SLR modes with three energies along different in-plane directions. The dark green, light green, and orange concentric circles indicate the light-cone cross sections at three energies at the  $\Delta$ ,  $\Sigma$ , and X points, respectively. The dots on the concentric circles indicate the light-cone SLR modes. (b) Band structure calculated using the coupled dipole method. An infinite array of spherical NPs (d=80 nm) was used in the calculations. The dark green, light green, and orange lines indicate three energy levels at the  $\Delta$ ,  $\Sigma$ , and X points. The dark green, light green, and orange circles indicate the band-edge SLR modes in the reduced BZ. (c-e) Calculated radiation intensity distribution at the  $\Delta$ ,  $\Sigma$ , and X points. The dark green, light green, and orange circles indicate the light cones at E=2.37 eV, E=2.23 eV, E=2.11 eV respectively. The unit of the intensity in (c-e) is  $\frac{\sqrt{e_r}\omega^4 |p|^2}{12\pi e_0c^3N^2}$ .

plane scattering spectra can possibly be measured using a passive method with a broadband light source, our active method based on lasing exhibits orders of magnitude higher light intensity and can selectively capture the photonic modes only at the band edges.

Figure 4a depicts light-cone SLR modes at the third, fourth, and fifth BZ edges based on the intersections of the light-cone boundary and the high-order BZ edges in Figure 1c. Because of the symmetry of the high-order BZs, these modes show multiple in-plane radiation directions along different azimuthal angles. After being folded back into the first BZ, the light-cone modes at the third, fourth, and fifth zone edges are at the X ( $\mathbf{k}_{\parallel} = \frac{1}{2}\mathbf{b}_{1}$ ),  $\Sigma$  ( $\mathbf{k}_{\parallel} = \frac{1}{6}\mathbf{b}_{1} + \frac{1}{6}\mathbf{b}_{2}$ ), and  $\Delta$  ( $\mathbf{k}_{\parallel} = \frac{1}{4}\mathbf{b}_{1}$ ) points, respectively. Because connections between the localized fields and radiated fields are now possible using our coupled dipole radiation theory (Supporting Information Section 2), all radiated fields can now be predicted based on the high-symmetry points in the irreducible BZ of the localized fields ( $\Gamma$ - X - M -  $\Gamma$  triangular area, Figure 4a).

We labeled the three band-edge SLR modes at E=2.37, 2.23, and 2.11 eV on the calculated SLR band structure (Figure 4b, Figure S5). Using these photon energies and their wavevectors, we calculated the radiation intensity distributions of the three sets of optical modes and plotted their projections on the  $\mathbf{k}_{\parallel}$  plane (Figure 4c–e, Figures S6–8). Although the radiated fields are in 3D space outside the lattice, their projection on the 2D reciprocal plane reflects the symmetry of the photonic structure. For example, at E=2.37 eV, the four radiated beams from the  $\Delta$  points inside the first BZ form a unit cell, and  $\mathbf{k}_{\parallel}$  of all of the beams within the light cone show a periodicity of  $2\pi/a_0$  along the  $k_x$  and  $k_y$  directions (Figure 4c).

Similar periodic features of SLR modes are observed at  $E=2.23~{\rm eV}~(\Sigma~{\rm point})$  and  $E=2.11~{\rm eV}~(X~{\rm point})$  (Figure 4d,e). The different radiation intensity distributions are determined by the locations of the high-symmetry points in the first BZ. Note that the combination of the square lattice symmetry and circular light-cone cross sections results in multiple degenerate band-edge SLR modes on the light-cone boundary. Based on the analysis of 1D, 2D, and 3D lattices (Figure S9), we also revealed that the dimensionality of a photonic lattice affects the radiation intensity distribution because of interference from the scattered light from each nanoparticle.

Probing the high-order BZs of photonic lattices experimentally is challenging because multidirectional light scattering at high-order diffraction modes has large losses.<sup>2,32</sup> To investigate the third to fifth BZ edges, we fabricated 2D square arrays of aluminum nanoparticles with increased periodicity ( $a_0$ = 450 nm, d = 80 nm, h = 60 nm) on fused silica (Figure 5a). Different from the  $a_0 = 225$  nm system, we used C481 dye molecules as the local dipole sources because their broad PL emission spectrally overlaps all three light-cone SLR wavelengths. Using a 400 nm fs-pulsed laser to pump the dye, we obtained in-plane lasing emission with three different colors simultaneously (Figure 5b, Figure S10). By rotating the lattice, different lasing colors were selectively captured by the detector (Figure 5c). 522 nm lasing from the  $\Delta$  point was at  $\varphi = 0^{\circ}$ ; 553 nm lasing from the  $\Sigma$  point was at  $\varphi = 8^{\circ}$ ; and 585 nm lasing from the X point was at  $\varphi = 27^{\circ}$  (Figure 5d), in agreement with the angles predicted in Figure 3a. The stretched shapes of the in-plane lasing beams (Figure 5b) are consistent with theory, where the radiated beams show larger divergence angles at larger  $\theta$  (Figure S8); this radiation property is a signature of the 2D lattice symmetry (Figures S9).

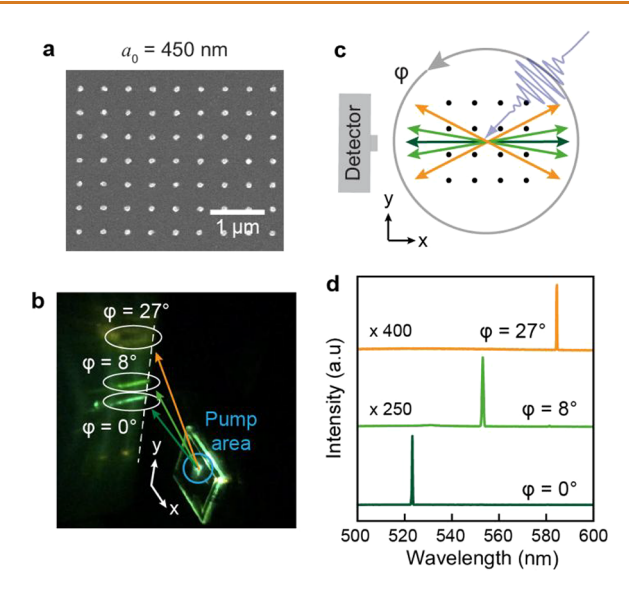


Figure 5. Tunable lasing wavelength through in-plane rotation of plasmonic lattices. (a) Scanning electron microscope image of aluminum nanoparticle lattices. The periodicity is 450 nm. (b) Photo of emission beams. (c) Scheme of lasing emission directions and color tuning by lattice rotation. (d) Lasing spectra at different in-plane rotation angle under a pump energy of 1.58 mJ/cm<sup>2</sup>.

We note that since dye emission is sensitive to pump polarization,<sup>30,31</sup> lasing emission from all possible cavity modes requires high pump powers (Figure 5b, Figure S11) or the rotation of the pump polarization.

# **CONCLUSIONS**

In summary, we directly identified high-order BZ edges in photonic lattices by leveraging light-cone SLR modes. This work provides critical insight into how plasmonic nanoparticles enable investigations of radiative losses (not easily observed with nonplasmonic lattices) because of their subwavelength light confinement and strong scattering. We revealed that extended BZs of a photonic lattice can account for both localized fields inside the lattice and radiated fields in the surroundings. Furthermore, these extended BZs in combination with the light cone provide an intuitive geometric method to design light-cone SLRs modes that can support in-plane lasing emission at multiple wavelengths and angles for on-chip applications. Our studies of photonic BZ edges in plasmonic lattices offer a design strategy to realize real-time tunable lasing wavelengths from a single architecture by lattice rotation, which is not possible in traditional lasers.

# **METHODS**

Fabrication of Aluminum Nanoparticle Lattices. Al nanoparticle lattices were fabricated with a soft nanofabrication process. First, periodic photoresist posts were generated on Si wafers by solvent-assisted nanoscale embossing (SANE<sup>27</sup>). Next, 8 nm of Cr was deposited on the Si substrate by thermal evaporation followed by the removal of the photoresist posts. After deep reactive ion etching to create cylindrical Si pits beneath the circular Cr holes (depth ∼200 nm), a hole array in a Au film was obtained by depositing 100 nm of Au on the Cr−Si hole array. Wet etching of the Cr adhesion layer released the Au hole film from the Si, which was then used as a deposition mask to create plasmonic nanoparticle lattices (area ∼0.5 cm²). Al nanoparticles were deposited by e-beam evaporation through the Au hole-array mask on a fused silica substrate; the deposition mask was removed using adhesive tape.

Lasing Measurements. A drop of DCM or C481 dye dissolved in DMSO was sandwiched between the nanoparticle lattice and glass coverslip. The sample was mounted on a rotational holder so that the angle of the lattice relative to the detector could be controlled. Dyes were optically pumped using 35 fs, 400 nm laser pulses with a repetition rate of 100 Hz, and the circular pump spot size was ~500  $\mu$ m in diameter. The 400 nm laser pulses were generated by directing the 800 nm output from a Ti: sapphire laser into a  $\beta$  barium borate (BBO) crystal to produce the doubled frequency of 400 nm pulses. The pump energy was controlled using a variable neutral density filter. Pulsed laser emission was collected at the edge of the sample with a free space distance from the sample of several centimeters. Far-field emission spectra were captured using a spectrometer and a charged coupled device (CCD) camera. The resolution of the spectrometer is 0.1 nm.

# **ASSOCIATED CONTENT**

# Supporting Information

The Supporting Information is available free of charge at https://pubs.acs.org/doi/10.1021/acsnano.1c00449.

Projection of light cone on extended BZs; coupled dipole radiation theory for photonic lattices; light-cone SLR mode at the X point of the first BZ; lasing threshold behavior and polarization; measured SLR band structure; radiated fields under different dipole orientations; dependence of radiation intensity distributions on the number of nanoparticles; radiation intensity distributions in  $(\theta, \varphi)$  space; light radiation properties of 1D, 2D, and 3D lattices; power-dependent lasing spectra (PDF)

# **AUTHOR INFORMATION**

#### **Corresponding Authors**

George C. Schatz – Graduate Program in Applied Physics and Department of Chemistry, Northwestern University, Evanston, Illinois 60208, United States; ⊚ orcid.org/0000-0001-5837-4740; Email: g-schatz@northwestern.edu

Teri W. Odom — Graduate Program in Applied Physics, Department of Chemistry, and Department of Materials Science and Engineering, Northwestern University, Evanston, Illinois 60208, United States; orcid.org/0000-0002-8490-292X; Email: todom@northwestern.edu

#### **Authors**

Jun Guan – Graduate Program in Applied Physics, Northwestern University, Evanston, Illinois 60208, United States; © orcid.org/0000-0001-8667-1611

Marc R. Bourgeois — Department of Chemistry, Northwestern University, Evanston, Illinois 60208, United States; orcid.org/0000-0002-9435-9051

Ran Li — Department of Materials Science and Engineering, Northwestern University, Evanston, Illinois 60208, United States; © orcid.org/0000-0001-5606-3826

Jingtian Hu — Department of Chemistry, Northwestern University, Evanston, Illinois 60208, United States;
orcid.org/0000-0002-0528-6250

Richard D. Schaller — Department of Chemistry,
Northwestern University, Evanston, Illinois 60208, United
States; Center for Nanoscale Materials, Argonne National
Laboratory, Lemont, Illinois 60439, United States;
orcid.org/0000-0001-9696-8830

Complete contact information is available at: https://pubs.acs.org/10.1021/acsnano.1c00449

# **Author Contributions**

J.G. and T.W.O. conceived the idea of light-cone SLR modes at high-order BZ edges. J.G. developed the geometric method to predict light-cone SLR modes, fabricated the plasmonic nanoparticle lattices, and performed the lasing measurements. M.R.B. and J.G. developed the coupled dipole radiation theory, wrote the code, and carried out the calculations. R.L. and R.D.S. contributed to the lasing measurements. J.H. contributed to the coding. T.W.O., G.C.S., and R.D.S. guided the experimental and theoretical investigations. J.G., M.R.B., G.C.S., and T.W.O. analyzed the data and wrote the manuscript. All authors commented on and revised the manuscript.

#### **Notes**

The authors declare no competing financial interest.

# **ACKNOWLEDGMENTS**

We thank Dr. Charles Cherqui for helpful discussions. This work was supported by the National Science Foundation (NSF) under DMR-1904385 (J.G., M.R.B., G.C.S., and T.W.O.) and the Vannevar Bush Faculty Fellowship from DOD under N00014-17-1-3023 (J.G., R.L., J.H., and T.W.O.). Use of the Center for Nanoscale Materials, an Office of Science user facility, was supported by the U.S. Department of Energy, Office of Science, Office of Basic Energy Sciences, under Contract No. DE-AC02-06CH11357 (R.D.S). This work used the Northwestern University Micro/Nano Fabrication Facility (NUFAB), which is partially supported by Soft and Hybrid Nanotechnology Experimental (SHyNE) Resource (NSF ECCS-2025633), the Materials Research Science and Engineering Center (MRSEC) (DMR-1720139), the State of Illinois, and Northwestern University. This work made use of the EPIC facilities of Northwestern University's NUANCE Center, which has received support from the SHyNE Resource (NSF ECCS-2025633), the MRSEC program (NSF DMR-1720139) at the Materials Research Center, the International Institute for Nanotechnology (IIN), the Keck Foundation, and the State of Illinois through the IIN. This research was supported in part by the Quest high performance computing facility at Northwestern University, which is jointly supported by the Office of the Provost, the Office for Research, and Northwestern University Information Technology. This work made use of the Pritzker Nanofabrication Facility part of the Pritzker School of Molecular Engineering at the University of Chicago, which receives support from SHyNE Resource (NSF ECCS-2025633), a node of the National Science Foundation's National Nanotechnology Coordinated Infrastructure.

# **REFERENCES**

- (1) Schwarze, M.; Tress, W.; Beyer, B.; Gao, F.; Scholz, R.; Poelking, C.; Ortstein, K.; Gunther, A. A.; Kasemann, D.; Andrienko, D.; Leo, K. Band Structure Engineering in Organic Semiconductors. *Science* **2016**, 352, 1446–1449.
- (2) Joannopoulos, J. D.; Johnson, S. G.; Winn, J. N.; Meade, R. D. *Photonic Crystals: Molding the Flow of Light*, 2nd ed.; Princeton University Press: Princeton, 2008; pp 1–286.
- (3) Ashcroft, N. W.; Mermin, N. D. Solid State Physics; Saunders College: Philadelphia, 1976; pp 130–190.
- (4) Lourtioz, J.-M.; Benisty, H.; Berger, V.; Gerard, J.-M.; Maystre, D.; Tchelnokov, A. *Photonic Crystals*; Springer: Berlin, 2005; pp 5–102.
- (5) Inoue, K.; Ohtaka, K. Photonic Crystals: Physics, Fabrication and Applications; Springer: Berlin, 2004; pp 1-130.

- (6) Barnes, W. L.; Dereux, A.; Ebbesen, T. W. Surface Plasmon Subwavelength Optics. *Nature* **2003**, *424*, 824–830.
- (7) Barnes, W. L. Surface Plasmon-Polariton Length Scales: A Route to Sub-Wavelength Optics. *J. Opt. A: Pure Appl. Opt.* **2006**, *8*, S87—S93.
- (8) Krauss, T. F.; De la Rue, R. M. Photonic Crystals in the Optical Regime Past, Present and Future. *Prog. Quantum Electron.* **1999**, 23, 51–96.
- (9) Baba, T. Slow Light in Photonic Crystals. *Nat. Photonics* **2008**, *2*, 465–473.
- (10) Joannopoulos, J. D.; Villeneuve, P. R.; Fan, S. H. Photonic Crystals: Putting a New Twist on Light. *Nature* **1997**, 386, 143–149.
- (11) Kurosaka, Y.; Iwahashi, S.; Liang, Y.; Sakai, K.; Miyai, E.; Kunishi, W.; Ohnishi, D.; Noda, S. On-Chip Beam-Steering Photonic-Crystal Lasers. *Nat. Photonics* **2010**, *4*, 447–450.
- (12) Imada, M.; Chutinan, A.; Noda, S.; Mochizuki, M. Multidirectionally Distributed Feedback Photonic Crystal Lasers. *Phys. Rev. B: Condens. Matter Mater. Phys.* **2002**, *65*, 195306.
- (13) Zou, S. L.; Janel, N.; Schatz, G. C. Silver Nanoparticle Array Structures That Produce Remarkably Narrow Plasmon Lineshapes. *J. Chem. Phys.* **2004**, *120*, 10871–10875.
- (14) Auguie, B.; Barnes, W. L. Collective Resonances in Gold Nanoparticle Arrays. *Phys. Rev. Lett.* **2008**, *101*, 143902.
- (15) Kravets, V. G.; Kabashin, A. V.; Barnes, W. L.; Grigorenko, A. N. Plasmonic Surface Lattice Resonances: A Review of Properties and Applications. *Chem. Rev.* (Washington, DC, U. S.) **2018**, 118, 5912–5951
- (16) Wang, W. J.; Ramezani, M.; Väkeväinen, A. I.; Törmä, P.; Rivas, J. G.; Odom, T. W. The Rich Photonic World of Plasmonic Nanoparticle Arrays. *Mater. Today* **2018**, *21*, 303–314.
- (17) Zhou, W.; Dridi, M.; Suh, J. Y.; Kim, C. H.; Co, D. T.; Wasielewski, M. R.; Schatz, G. C.; Odom, T. W. Lasing Action in Strongly Coupled Plasmonic Nanocavity Arrays. *Nat. Nanotechnol.* **2013**, *8*, 506–511.
- (18) Fernandez-Bravo, A.; Wang, D. Q.; Barnard, E. S.; Teitelboim, A.; Tajon, C.; Guan, J.; Schatz, G. C.; Cohen, B. E.; Chan, E. M.; Schuck, P. J.; Odom, T. W. Ultralow-Threshold, Continuous-Wave Upconverting Lasing from Subwavelength Plasmons. *Nat. Mater.* **2019**, *18*, 1172–1176.
- (19) Guan, J.; Sagar, L. K.; Li, R.; Wang, D. Q.; Bappi, G.; Wang, W. J.; Watkins, N.; Bourgeois, M. R.; Levina, L.; Fan, F. J.; Hoogland, S.; Voznyy, O.; de Pina, J. M.; Schaller, R. D.; Schatz, G. C.; Sargent, E. H.; Odom, T. W. Quantum Dot-Plasmon Lasing with Controlled Polarization Patterns. *ACS Nano* **2020**, *14*, 3426–3433.
- (20) Guo, R.; Nečada, M.; Hakala, T. K.; Väkeväinen, A. I.; Törmä, P. Lasing at K Points of a Honeycomb Plasmonic Lattice. *Phys. Rev. Lett.* **2019**, *122*, 013901.
- (21) Guan, J.; Sagar, L. K.; Li, R.; Wang, D. Q.; Bappi, G.; Watkins, N. E.; Bourgeois, M. R.; Levina, L.; Fan, F. J.; Hoogland, S.; Voznyy, O.; de Pina, J. M.; Schaller, R. D.; Schatz, G. C.; Sargent, E. H.; Odom, T. W. Engineering Directionality in Quantum Dot Shell Lasing Using Plasmonic Lattices. *Nano Lett.* **2020**, *20*, 1468–1474.
- (22) Li, R.; Bourgeois, M. R.; Cherqui, C.; Guan, J.; Wang, D.; Hu, J.; Schaller, R. D.; Schatz, G. C.; Odom, T. W. J. N. l. Hierarchical Hybridization in Plasmonic Honeycomb Lattices. *Nano Lett.* **2019**, 19, 6435–6441.
- (23) Guo, R.; Hakala, T. K.; Törmä, P. Geometry Dependence of Surface Lattice Resonances in Plasmonic Nanoparticle Arrays. *Phys. Rev. B: Condens. Matter Mater. Phys.* **2017**, *95*, 155423.
- (24) Cherqui, C.; Bourgeois, M. R.; Wang, D. Q.; Schatz, G. C. Plasmonic Surface Lattice Resonances: Theory and Computation. *Acc. Chem. Res.* **2019**, *52*, 2548–2558.
- (25) Iwahashi, S.; Kurosaka, Y.; Sakai, K.; Kitamura, K.; Takayama, N.; Noda, S. Higher-Order Vector Beams Produced by Photonic-Crystal Lasers. *Opt. Express* **2011**, *19*, 11963–11968.
- (26) Kittel, C.; McEuen, P. Introduction to Solid State Physics; Wiley: New York, 1976; pp 23-46.

- (27) Lee, M. H.; Huntington, M. D.; Zhou, W.; Yang, J.-C.; Odom, T. W. Programmable Soft Lithography: Solvent-Assisted Nanoscale Embossing. *Nano Lett.* **2011**, *11*, 311–315.
- (28) Henzie, J.; Kwak, E. S.; Odom, T. W. Mesoscale Metallic Pyramids with Nanoscale Tips. *Nano Lett.* **2005**, *5*, 1199–1202.
- (29) Gao, H.; Henzie, J.; Odom, T. W. Direct Evidence for Surface Plasmon-Mediated Enhanced Light Transmission through Metallic Nanohole Arrays. *Nano Lett.* **2006**, *6*, 2104–2108.
- (30) Knudson, M. P.; Li, R.; Wang, D. Q.; Wang, W. J.; Schaller, R. D.; Odom, T. W. Polarization-Dependent Lasing Behavior from Low-Symmetry Nanocavity Arrays. ACS Nano 2019, 13, 7435–7441.
- (31) Wang, D.; Yang, A.; Wang, W.; Hua, Y.; Schaller, R. D.; Schatz, G. C.; Odom, T. W. Band-Edge Engineering for Controlled Multi-Modal Nanolasing in Plasmonic Superlattices. *Nat. Nanotechnol.* **2017**, *12*, 889–894.
- (32) Noda, S.; Baba, T. Roadmap on Photonic Crystals; Springer: Boston, 2013; pp 1-255.